Int J Biometeorol (1994) 38:5–17

REVIEW ARTICLE

Manuel Nunez · Bruce Forgan · Colin Roy

Estimating ultraviolet radiation at the earth's surface

Received: 19 September / Accepted: 25 September 1993

Abstract Surface ultraviolet (UV) irradiance depends not only on stratospheric ozone amounts, but also varies with time and date, latitude, cloud amount and aerosol load. Any assessment of the effect of stratospheric ozone depletion on surface UV irradiance must take into consideration all of the above parameters. Measurements in the UV-B region may be accomplished using filter and detector combinations which mimic a biological response curve. However there are uncertainties such as in determining the exact filter response and in the cosine error of the detector. The UV-A region lacks a strong ozone absorption band and approaches which relate measured UV-A irradiance to measured global irradiance show promise. Theoretical models have been derived which calculate spectral UV irradiance in cloudless and cloudy conditions. Results show that cloud transmissivities increase as wavelength increases; however, there is a strong dependence on cloud type. In the absence of surface observations of clouds, satellite data may be used to map UV-A and UV-B irradiance in a region, and this approach is illustrated using two specific examples.

Key words UV-A – UV-B – Earth surface radiation – Satellite assessment

Introduction

Amongst the various anthropogenic effects on the global climate, the role of ozone depletion is of particular concern. Early measurements, both surface and satellite based, revealed an increasing trend of high ozone depletion in Antarctica during the spring months (Stolarski et al. 1986; Farman et al. 1985). It appears that anthropogenic chlorine compounds, transported into the antarctic atmosphere, are largely to blame for this effect (Farman et al. 1985; Farmer et al. 1987; Fraser 1989), although other processes such as volcanic emissions (Angell et al. 1985; Hofman et al. 1992) and solar activity (Crutzen et al. 1975) are also important. More recent studies have confirmed that ozone depletion is not confined to Antarctica but that it is a global phenomenon which intensifies in polar regions (Atkinson et al. 1989; Lehman et al. 1992a, b). Recent figures obtained from satellite data give the yearly springtime depletion which is substantial at high latitudes, ranging from 3%/year for 80° S to 1% year for 80° N. Typical midlatitude figures are 0.3%/year and 0.8%/year for the spring months at latitudes 40° S and 40° N respectively (Stolarski et al. 1992).

Given the important role of ozone in blocking ultraviolet radiation, it is expected that any drop in stratospheric ozone will affect the levels of ultraviolet irradiance received at the earth's surface. In turn these changed levels could have significant consequences on human health and biological productivity (Zigman 1977; Worrest 1982; Scotto and Fears 1987; Hollows 1989). Despite the urgent need for these data, systematic global measurements of surface ultraviolet radiation are not available to examine this hypothesis. Isolated spectral measurements in Antarctica (Lubin and Frederick 1989, 1990; Frederick and Alberts 1991) and New Zealand (Seckmeyer and McKenzie 1992) confirm an increase in ultraviolet irradiance, which is related to lower ozone levels. By contrast, no increasing trend is reported at eight locations in the United States over a 12-year period from 1974 to 1985 (Scotto et al. 1988).

Using global ozone data from Stolarski et al. (1991), Madronich (1992) derived theoretical estimates of ultraviolet irradiance increases for various biologically active bands in the ultraviolet spectrum. His treatment includ-

M. Nunez (✉)
Department of Geography and Environmental Studies,
University of Tasmania, GPO Box 252C,
Hobart, Tas. 7001, Australia

B. Forgan
Bureau of Meteorology, GPO Box 1289K,
Melbourne, Vic. 3001, Australia

C. Roy
Australian Radiation Laboratory, Lower plenty Road,
Yallambie, Vic. 3085, Australia

ed Rayleigh scattering and ozone absorption, but no depletion by aerosols or clouds. Madronich argues that these increases, which typically reach values of 5 to 10% at latitude 45° S in spring, are independent of cloud or aerosols *provided these remain constant in time.* Although this analysis presents much useful information, it cannot either estimate absolute surface irradiance or account for interannual cloud and aerosol changes.

Many of the above uncertainties could be eliminated by the development of suitable regional and global climatology for surface ultraviolet radiation, which presently is unavailable due to several obstacles. These include a lack of universally acceptable instrumentation and the supporting measurement network, uncertainties of which spectral bands to cover, and lack of process studies to investigate depletion of ultraviolet radiation by atmospheric constituents such as cloud and aerosols. The purpose of this paper is to consider some of these points and suggest approaches which might prove useful in the future.

Measurement schemes

Figure 1 shows various components of relevance to surface measurement schemes. Most of the solar radiation at wavelengths less than 280 nm, in the ultraviolet C (UV-C) region, is absorbed in the atmosphere so that only very small amounts reach the earth's surface. Stratospheric ozone, typically some 3 mm thick at surface pressures but extending through 30 km of stratospheric altitudes, is the main absorption mechanism (Barton and Paltridge 1979). Some of the ultraviolet radiation in the wavelength range 280–320 nm, the UV-B region, reaches the earth's surface with actual amounts depending on the air mass depth of ozone, Rayleigh scatter, and cloud and aerosol content. Very low levels of ozone absorption occur at wavelengths greater than 320 nm, the UV-A region.

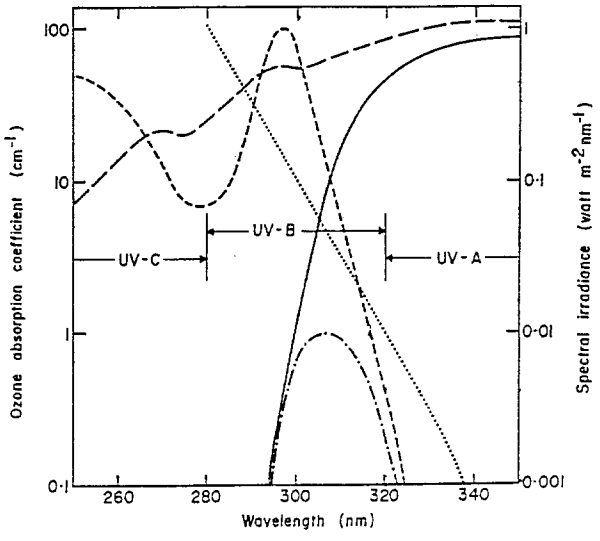

Fig. 1 Ozone absorption coefficient, erythemal response of human skin and solar irradiances for the middle ultraviolet (after Barton and Paltridge 1979). – – – – Spectral irradiance outside the atmosphere; ——— typical spectral irradiance at the earth's surface; ····· ozone absorption coefficient; - - - - - erythemal response of human skin; —·—·— typical erythemal dose at the earth's surface

On a cloudless day ultraviolet radiation will form between 3 and 5% of the total surface irradiance (Iqbal 1983). This does not represent a large amount in the surface radiative budget and existing pyranometer measurements include an ultraviolet component as part of the broadband solar radiation estimate. The need for surface ultraviolet radiation data is apparent in specific applications which may link radiation levels to some form of damage to biological organisms at the earth's surface. Such damage is usually very specific spectrally and requires only a portion of the total ultraviolet spectrum. In the most general case, spectral irradiance may be obtained for the entire range of ultraviolet radiation. The preferred assembly consists of an optical head with a diffusing plate and a good cosine response; a fibre optic probe may provide a wide range of viewing angles. The signal is separated in a double monochromator with a spectral resolution usually of 1 nm, and subsequently fed into a photomultiplier tube for amplification. The final step involves collection of digital data with either a digital voltmeter or computer (Seckmeyer and McKenzie 1992; Lubin and Frederick 1989; Kok et al. 1978).

Spectral measurements made with the above instrumentation are of crucial importance in a wide range of applications. Essentially they provide high quality data which may be used to observe physical processes and their rate of change, to validate spectral irradiance models, and to calibrate broadband radiometers. It may be argued that the instruments are too costly and the data too voluminous for routine climatological measurements. In some applications the data have been convolved with the erythemal action spectrum (McKenzie et al. 1991), thus obtaining ultraviolet erythemal radiation. Other applications reduce the data considerably by using only noontime irradiance ratios between two bands in the ultraviolet (Frederick and Alberts 1991; Lubin and Frederick 1989). The ratio is highly dependent on ozone changes if one band and not the other is chosen in a region of high absorption. The authors argue that cloud depletion is non-wavelength selective in the UV band and therefore the ratio should cancel any cloud effect.

The Eppley Laboratory Solar and Sky Ultraviolet Radiometer has been used to measure radiation in the UV-A region (Blumthaler and Ambach 1988; Baker-Blocker et al. 1980, 1984; Rodskjer 1983). The instrument consists of a selenium photocell detector with a diffusing plate and band pass filters. The maximum response is at 345 nm with a half band width of ± 25 nm (Drummond and Wade 1969). The photocell response is wavelength-dependent and errors may arise in estimating the UV-A irradiance. The objective is to relate the

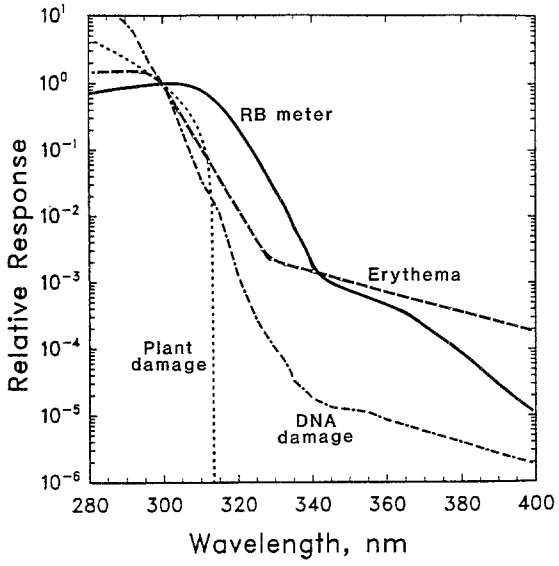

Fig. 2 Action spectra for the computation of effective ultraviolet radiation doses (after Madronich 1992)

instrument signal to the integrated spectral irradiance in the UV-A band. Denoting K_λ as the spectral irradiance, C the calibration constant and B an instrument constant, the relationship is (Rodskjer 1983):

$$\int_{290}^{385} K_\lambda \partial\lambda = CB \int_{290}^{385} K_\lambda F_\lambda \partial\lambda \quad (1)$$

where F_λ is the instrument spectral response given as the product of the filter and detector response function. A good calibration factor C is independent of K_λ, which may vary with solar angle and atmospheric opacity though in actual fact C is dependent on these variables (Rodskjer 1983).

A practical way of obtaining ultraviolet irradiance data is to define the biological region of interest by means of the 'action spectrum'. It is defined as a spectral sensitivity curve, usually normalised to 1 at the wavelength of maximum sensitivity. Three curves have been used in the literature: one corresponding to erythema induction in humans or reddening of the skin (McKinlay and Diffey 1987), a curve representing generalised DNA damage (Setlow 1974), and a third representing plant damage (Caldwell et al. 1986); Fig. 2 shows the respective characteristics. Taking the erythemal curve ($F_{\lambda E}$) as an example, the erythema irradiance is:

$$K_m = \int_{290}^{385} K_\lambda F_{\lambda E} \partial\lambda \quad (2)$$

At a wavelength of 300 nm $F_{\lambda E}$ equals 1 and radiation energy is used most efficiently in skin burning. At a larger wavelength the efficiency is lower and more energy is needed to produce the same effect. Therefore K_m defines the total irradiance as relevant to skin burning in humans.

The Robertson-Berger meter (Berger 1976; Paltridge and Barton 1978) mimics the erythemal irradiance described in Eq. 2 (see also Fig. 2). The instrument consists of a UV filter which blocks the visible and infrared radiation. A phosphor layer is sensitive to ultraviolet radiation with a response curve similar to the erythemal response of human skin. Once sensitised, the phosphor layer re-radiates in the visible/green band and the signal is furthered filtered and finally detected by a photodiode. The instrument is read in counts, with 440 counts producing a 'sunburn unit'. In turn this unit "equals a minimal erythema dose (MED) when untanned human skin is exposed to a vertical tropical sun .... This assumes average untanned Caucasian skin, sea level overhead sun in a clear sky and stratospheric ozone of 2.6 mm" (Berger and Urbach 1982). Basher (1987) applied the model of Green et al. (1974b) in Eq. 2 to derive an energy value of 207 J/m^2 (300 nm equivalent) for the sunburn unit. However a wide range of values have been reported in the literature (Basher 1987).

Other similar broadband instruments have been used to measure various regions of the ultraviolet spectrum (Roy et al. 1989; Webb and Steven 1984). One commercial instrument (International Light) features an NS 297 filter designed for monitoring the erythemal 296.7 nm wavelength with spectral half power points of 288 nm and 300 nm and an SED 240 solar blind vacuum photodiode (which accepts wavelengths of 200–320 nm). Other filter/sensor combinations may be used for other regions of the ultraviolet spectrum. A reliable calibration may be obtained with knowledge of the filter/detector spectral response, the cosine response of the optical head and by comparing signal output with spectral irradiance data (Grainger et al. 1993). Calibration errors due to radiation/filter spectral characteristics (Eq. 1) are avoided by choosing a filter/detector response to match the desired biological action spectrum.

Many applications may require the personal exposure of a human being in a variety of activities. This information may be most easily obtained using photosensitive film attached to the individual. Polymer polysulphone when used as a thin film deteriorates after exposure to UV-B radiation. The degree of deterioration is determined by the increase in optical absorbance at 330 nm and this value can then be related to UV-B dosage (Roberts 1991). The advantages of the above technique are considerable such as ease of handling, usefulness in difficult environments and relatively low cost. On the negative side there are problems in matching the spectral sensitivity of the film with the erythemal curve, film reproducibility and occurrence of dark reactions after exposure (Davis et al. 1976). Given the nature of the measurement, very short time intervals of exposure might cause the film to be underdeveloped, with the opposite effect occurring at long time intervals (P. Gies, personal communication).

Personal dosimetry can play a useful and significant role in determining human radiation loads. Nevertheless, it is important to keep a perspective on the spatial scales involved. Photodiodes with suitable filters may be used to provide measurements of the regional irradiance

Table 1 Trends in annual integral of ozone and ultraviolet radiation, expressed as percentage change over 10 years, 1979–1989 (after Madronich 1992)

Latitude	Total ozone	RB meter	Erythema induction	Plant damage	DNA damage
85 N	− 4.5±3	5.1±1.5	4.7±1.4	14.8± 4.3	10.1± 3.2
75 N	− 4.5±2.7	3.9±1.3	4.1±1.4	10.8± 3.4	9.0± 2.9
65 N	− 4.2±1.7	3.4±1.3	4.0±1.5	8.9± 3.3	8.1± 3.0
55 N	− 4.4±1.2	3.3±1.2	4.0±1.5	8.1± 3.0	7.7± 2.9
45 N	− 4.5±1.0	3.1±1.0	4.0±1.4	7.2± 2.6	7.2± 2.7
35 N	− 4.5±1.3	3.0±1.1	4.3±1.6	7.0± 2.7	7.5± 3.0
25 N	− 2.7±1.6	1.8±1.1	2.8±1.9	4.2± 2.8	4.8± 3.3
15 N	− 0.7±1.2	0.5±0.8	0.8±1.4	1.1± 1.9	1.3± 2.3
5 N	− 1.2±1.4	0.8±1.0	1.3±1.6	1.8± 2.3	2.2± 2.7
5 S	− 1.2±1.3	0.8±0.8	1.3±1.4	1.8± 2.0	2.1± 2.4
15 S	− 0.3±1.2	0.2±0.8	0.4±1.3	0.6± 1.8	0.7± 2.2
25 S	− 1.2±1.7	1.0±1.1	1.8±1.7	2.7± 2.5	3.3± 2.8
35 S	− 3.1±1.7	2.3±1.1	3.5±1.6	5.6± 2.6	6.3± 2.9
45 S	− 4.9±1.5	3.7±1.1	5.3±1.6	9.3± 2.8	9.9± 3.0
55 S	− 7.3±1.7	6.0±1.5	7.7±1.9	15.4± 4.0	15.1± 3.9
65 S	−10.8±2.2	9.5±2.3	11.4±2.8	25.4± 6.6	23.4± 6.1
75 S	−13.2±2.8	12.8±3.9	15.0±4.8	39.0±13.4	34.4±11.9
85 S	−14.5±3.4	15.6±5.1	16.8±5.7	53.9±20.2	42.7±15.8

developing from a combination of solar zenith angle, ozone content, cloud cover and aerosol load. Localised effects arising from processes such as building and tree shadows and surface albedos modulate the regional pattern. Polysulphone badges may measure the local irradiance but these data need to be linked to the regional irradiance to be set into perspective.

The study of ultraviolet radiation and its impacts is a very complex field and most studies have concentrated on specific bands which are of interest for biological applications. Broadband measurements of the entire ultraviolet radiation spectrum are less biologically important and are heavily weighed towards the larger, more energetic wavelengths which are not sensitive to ozone absorption. In addition, broadband measurements with wavelength-sensitive detectors are subject to errors as has already been mentioned (Eq. 1). The data of Table 1 show decadal trends in surface UV-B irradiance after integration by the three action spectra (Madronich 1992), and emphasize the importance of the choice of spectral bands. Large differences occur in the changes, with highest values being obtained for the 'Plant damage' action spectra.

It appears that much work still needs to be done in defining an ultraviolet region of common interest, in developing a common instrument that is widely accepted, and in the provision of measurement standards. The three action spectra shown in Fig. 2 illustrate the importance of the UV-B region. In terms of developing surface climatologies, the Robertson-Berger meter appears to be the only one that has been uniformly used and has a suitably long record. However the calibration and long-term reliability aspects present problems, and the issue of a measurement standard still needs to be broached.

Modelling surface ultraviolet irradiance for clear skies

Various approaches have been attempted and are briefly discussed in this section. Halpern et al. (1974) and Dave and Halpern (1976) used a plane parallel atmosphere with a varying number of layers. Each layer was characterised by a value for ozone and an aerosol optical depth for a partially absorbing aerosol; surface albedo was also taken into account. The model expanded the radiant intensity as a Fourier series in the radiative transfer equation and a successive scattering iteration procedure was used to solve the resultant equation. The results were presented as spectral irradiance for varying levels of ozone content, aerosol absorption and aerosol concentration. Atmospheric transmission levels due to aerosols are highest at the short wavelengths (<300 nm) and decrease regularly with wavelength. Very little extra depletion is reported in the UV-B region for an atmosphere containing average aerosol concentrations.

Rao et al. (1984) also developed a vertically inhomogeneous model with 9 layers and variable amounts of ozone, aerosols (non-absorbing) and surface albedo. An adding method was used to compute the spectral irradiances at 19 wavelengths from 290 to 380 nm. Model predictions were found to depend substantially on the values used for the extra-terrestrial solar irradiance, while other errors were attributed to seasonal changes in aerosol loads. Frederick and Lubin (1988) and Frederick and Snell (1990) used a two-stream approximation model similar to Meador and Weaver (1980). The first paper used global data from the Nimbus 7 Solar Backscatter Ultraviolet Radiometer (SBUV) to arrive at a UV global radiation budget for the month of July. Their results showed enhanced absorption of UV-B radiation in the troposphere during cloud-covered conditions. The second paper also used a two-stream approximation, but with cloud data for four stations in the United States. These results will be described below in the section on clouds.

Two recent studies (Vogelmann et al. 1992; Liu et al. 1991) developed models to examine the effect of recent aerosol emissions on the magnitude of the UV-B irradiance at the earth's surface. Liu et al. (1991) used a radiative transfer model based on discrete ordinates with an evenly mixed tropospheric aerosol concentration. The results show a drop in UV-B irradiance levels of between 5 and 18% in non-urban regions of industrialised countries since industrialisation began. This drop will partly offset the expected UV-B increase due to stratospheric ozone depletion. Using a similar modelling framework, Vogelman et al. (1992) argue that recent volcanic eruptions from El Chichon (1982) and Mount Pinatubo (1991) decrease the UV-B irradiance at the surface due to scattering. However the effects of ozone depletion outweigh the increased scattering.

Madronich (1992) used a multi-layer delta Eddington radiative transfer scheme to estimate surface UV-B irradiance, which is integrated by various biological action spectra. No clouds or aerosols are considered and the surface albedo is maintained constant at 5%. Percentage changes in surface ultraviolet irradiance should be independent of the above variables provided these remain constant. The results of Madronich (1992) have already been presented in Table 1.

An alternative approach to the complex multiple scattering calculations has been developed by Green and coworkers at the University of Florida. The models are semi-empirical and are based on the solar UV-B spectral irradiances of Bener (1972) and model results of Braslau and Dave (1973a, b) and Dave and Halpern (1976). The relationships are optimised to reproduce the available data and have the capacity for interpolation or extrapolation to other sets of conditions (Green et al. 1974a, b, 1980; Schippnick and Green 1982; Rundel 1986). The model calculates the direct (S_λ) and diffuse irradiance (D_λ) as (Rundel 1986):

$$S_\lambda = I_{0\lambda} \cos(Z) \exp[-\sum \tau_i / \cos(Z)] \quad (3)$$

$$D_\lambda = \delta(\lambda, Z)\, M(\lambda)\, I(\lambda, 0) \quad (4)$$

where $I_{0\lambda}$ is the extra-terrestrial intensity, Z is the local zenith angle and τ_i represents optical depths for Rayleigh scatter, ozone absorption, aerosol scattering and aerosol absorption. The diffuse radiation D_λ is given in terms of the direct irradiance $I(\lambda, 0)$, for 0 degrees, zenith angle Z and functions $M(\lambda)$ and $\delta(\lambda, Z)$. These are defined as $M(\lambda) = S(\lambda, 0)/D(\lambda, 0)$ and $\delta(\lambda, Z) = S(\lambda, Z)/(S(\lambda, 0)$. In Eq. 4, I is expected to vary widely over the entire UV-B range. By contrast δ and M are well behaved empirical functions which are easily calculated (Rundel 1986).

Estimating surface ultraviolet irradiance for cloudy skies

Theoretical models. Nack and Green (1974) used a modified discrete ordinate model of Shettle and Green (1974) containing five layers in a standard atmosphere. A sixth layer was added to allow for clouds or haze. Cloud optical depths ranging from 0.1 to 100 were used. Data were presented as the ratio of a cloudy to a cloudless spectral irradiance for direct, diffuse and global radiation respectively:

$$T_{i\lambda} = I_\lambda / I_{0\lambda}$$

$$T_{D\lambda} = D_\lambda / D_{0\lambda}$$

$$T_{G\lambda} = [(I_\lambda \cos(Z) + D_\lambda)/(I_{0\lambda} \cos(Z) + D_{0\lambda})] \quad (5)$$

where I and D refer to direct beam intensity and diffuse irradiance for cloudy conditions and are defined at a discrete wavelength interval centred on λ. The subscript 0 refers to the corresponding cloudless case, and the transmissivity is expressed as T with the subscripts G, D and i standing for global, diffuse and direct radiation, respectively.

The results show that for low zenith angles and cloud optical depths less than 10, $T_{D\lambda}$ is greater than 1. For a given optical depth (τ), $T_{D\lambda}$ will be lower at the shorter wavelengths, $T_{G\lambda}$ is less than 1, and values are generally above 0.8 for cloud optical depths less than 1. For a partly cloudy sky, $T_{G\lambda}$ may be greater than 1 provided clouds do not obscure the direct beam, and for conditions $Z = 0$, $\tau < 1.0$ and cloud cover equal to 0.8. At the other extreme, for overcast conditions and with τ approximately equal to 100, $T_{G\lambda}$ and $T_{G\lambda}$ and $T_{D\lambda}$ are approximately 0.1 or less.

A later paper (Spinhirne and Green 1978) also used the model of Shettle and Green (1974) to investigate the ratio of the ultraviolet spectral irradiance to the total solar irradiance under uniform cloud layers of varying optical depths. The ratio decreases with Z and the authors attributed this effect to decreasing ozone optical depth. However, for a fixed Z, the ratio increases with cloud optical depth.

Halpern et al. (1974) extended their model (described earlier in the clear sky section) to include a stratus cloud layer. Estimates of $T_{G\lambda}$ with the inclusion of clouds dropped substantially. For low values of Z there is little dependence of $T_{G\lambda}$ on wavelength. For high Z, $T_{G\lambda}$ decreases with increasing wavelength. For average aerosol concentrations, stratus cloud and Z equal to 80°, $T_{G\lambda}$ ranges from 0.8 for $\lambda = 300$ nm to 0.68 for $\lambda = 400$ nm.

Surface estimates. In most cases, the large variabilities experienced in cloud properties and cloud distribution would rule out a strictly theoretical approach when mapping surface ultraviolet radiation. The above theoretical studies indicate that clouds are an important depletion agent, that the depletion is dependent on cloud optical depth and zenith angle, and that for a given set of conditions, the relative transmissivity is not independent of wavelength. For practical applications $T_{G\lambda}$ must be linked to surface measurements or cloud cover. In other studies, narrowband/broadband relationships have been developed. These approaches form the basis of the following discussion.

Frederick and Snell (1990) used daily irradiance from Robertson-Berger meters to calculate $T_{G\lambda}$ for four sites in the United States over a 1 year period. The monthly average irradiance and daily lowest irradiance were divided by the corresponding monthly clear sky value. Therefore mean and lowest cloud transmissivities were obtained. Mean transmissivities ranged from a minimum of 0.5 (Bismarck, N.D. in February) to 0.9 (El Paso, Texas in June). They also showed that in some cases cloud cover can wipe out latitudinal effects. If fractional cloud cover during June and July varied by $\pm 10\%$ of its monthly mean value, erythemal irradiance at the different sites would undergo changes from 1.2 to 6.4% with opposite sign.

Berner (1964) conducted very detailed estimates of $T_{G\lambda}$ for two wavelengths (330 nm, 370 nm), three cloud levels (low, middle and high) and varying cloud cover and zenith angle. The study was done at Davos, Switzerland. Mean $T_{G\lambda}$ values at 330 nm were 0.85, 0.70 and 1.10 for layers of low, middle and high clouds respectively in summer. Corresponding values for winter were 0.73, 0.91 and 1.10. In all cases the standard deviation was more than 22%, which points to the considerable variability in cloud transmission properties, even when grouping them according to cloud type and in near overcast conditions.

Blumthaler and Ambach (1988) measured $T_{G\lambda}$ for UV-A, UV-B (erythemal) and global radiation in Switzerland. All data were grouped in bins of 1/10 cloud cover and mean $T_{G\lambda}$ values were plotted against cloud cover. The results showed similar behaviour of $T_{G\lambda}$ for both UV-A and UV-B erythemal radiation. $T_{G\lambda}$ values decreased almost linearly with increasing cloud cover (C), reaching lowest values of around 0.6 when C equals 1. A similar approach has been developed by Reiter et al. (1982) and Baker-Blocker (1980) using sunshine duration instead of cloud cover data.

A relationship that has been used in the literature for UV-B radiation is:

$$T_{GE} = 1 - 0.56\, C \tag{6}$$

where T_{GE} denotes the ratio of cloudy sky to clear sky irradiance as measured by an erythemal radiometer. It was originally described in a paper by Green et al. (1974a) and used by Mo and Green (1974) to estimate daily and monthly erythemal radiation for 10 metropolitan areas in the United States. The relationship has been found to agree with UV-B measurements (Ilyas and Barton 1983) and UV-A measurements (Ilyas 1987) at Penang, Malaysia. However, Borkowski et al. (1974) using data from an Eppley ultraviolet radiometer and a Robertson-Berger meter found much scatter and little evidence of a linear T_{GE} versus C relationship. They subsequently investigated the use of all-sky cameras and empirical orthogonal function analysis to characterise the spatial field.

In trying to derive empirical relationships, it is important to consider the temporal scale chosen (Davies et al. 1975). At the high frequency scale, there will be problems in relating spatial cloud estimates with pyranometer point measurements. Cloud type, as measured by Berner (1964) also influences the transmissivity T_{GE} and as a result Eq. 6 may contain much scatter. It is only at temporal scales of a month or larger that simple linear relationships truly apply. The slope of the regression relationship (0.56 in the case of Eq. 6) incorporates all combinations of cloud type transmissivities peculiar to the individual climate. The results are useful but are empirical and therefore this relationship needs to be tested at various geographical locations and regions.

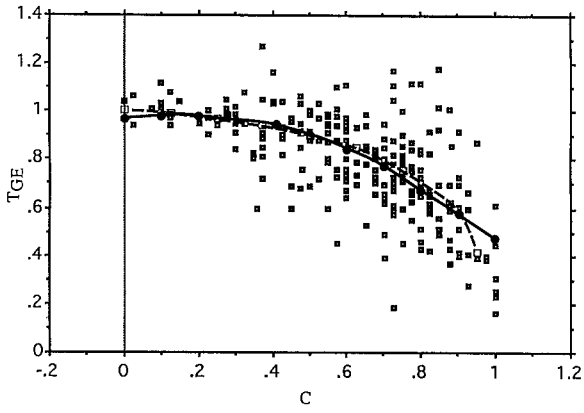

Fig. 3 Daily transmissivity of erythemal ultraviolet radiation (T_{GE}) versus mean daily cloud cover (C). Data were taken at Hobart, Australia between the period 1 March 1990 to 28 February 1990. The *heavy black line* represents a multiple regression fit using cloud cover. The *dashed line* represents best fit by eye from the data of Barton and Paltridge (1979)

On a daily scale it would appear that the T_{GE} cloud cover relationship is distinctly non-linear. Figure 3 shows daily cloud cover versus T_{GE} taken in Hobart, Australia for the period 1 March 1990 to 28 February 1991. Clear sky erythemal irradiances (K_{0E}) have been obtained using the relationship of Green et al. (1980) and have been further modified against clear sky measurements with an IL 1700 UV-B erythemal radiometer. The line of best fit gives the following relationship:

$$\begin{aligned} T_{GE} &= 0.967 + 0.223\, C - 0.721\, C^2 \\ r^2 &= 0.422 \\ \mathrm{SE} &= 0.161 \end{aligned} \tag{7}$$

For comparison, a T_{GE} curve obtained from Barton and Paltridge (1979) for Aspendale, Australia is also presented. The agreement between the two curves is good, indicating that despite the scatter there is some consistency in the mean patterns. There are a substantial number of days when T_{GE} is greater than 1 for low and medium cloud cover. Very likely these are days when the direct radiation as received by the radiometer sensor was not obscured by clouds, although surrounding cloud cover would enhance the diffuse radiation (Nack and Green 1974).

Another useful approach in the surface estimation of ultraviolet radiation is to seek relationships between measurements of narrowband ultraviolet radiation and

broadband solar radiation. The usefulness here is that solar radiation is more commonly measured and climatological estimates are available in many regions. Therefore this technique may yield long-term estimates of ultraviolet radiation provided the relationships are sufficiently general to encompass all possible conditions. Zavodska (1984) found for a clear day that UV-A irradiance varied between 4 and 7% of the broadband solar irradiance. This ratio increased to 8–11% for cloudy conditions. Similar results have been reported by Blumthaler and Ambach (1988) using the ratio of erythemal T_{GE} to broadband solar irradiance cloud transmissivities (T_{GS}) versus C. This ratio (T_{GE}/T_{GS}) was found to increase with C, therefore confirming the lower depletion of UV-B radiation by cloud cover.

Webb and Steven (1984) have related diffuse/global ratios in the UV-B region to corresponding ones in the visible band and the solar broadband. In a later paper (Webb and Steven 1986), the authors derive a linear regression between daily UV-B and daily global irradiance. The intercept was not statistically different from zero, but the slope was subject to differences on a monthly basis. These differences are minimised by normalising for ozone depletion and solar zenith angle. Comparisons of UV-B with global solar irradiances are obscured by strong ozone depletion at wavelengths less than 315 nm. A stronger relationship may be expected between UV-A and the broadband solar irradiance. To illustrate this relationship, data over two years (1985, 1986) of daily UV-A and broadband solar irradiances were used from the Cape Grim baseline station located in northwestern Tasmania. An Eppley UV pyranometer measured UV-A irradiance, whilst a Middleton CN27 pyranometer, calibrated to the World Radiation Reference (via the Australian Radiation Standards) measured broadband solar irradiance; no similar standards were available for the Eppley pyranometer. A long-term deterioration was noticed in the UV-A measurements at Cape Grim. The assumption was made that the ratio of UV-A to the broadband global radiation was constant and correctly described the 1977 value. This assumption allowed the correction of all subsequent UV-A data.

A linear regression between UV-A irradiance (K_{UVA}) and global solar irradiance (K_S) gave the following results (Fig. 4A):

$$K_{UVA} = 0.027 + 0.0374\ K_S$$
$$r^2 = 0.988$$
$$SE = 0.035 \qquad (8)$$

where the units of K_{UVA} and K_S are in MJ m^2 per day. Similar results have been reported in the literature (Baker-Blocker et al. 1984).

Further insight into the depletion process may be obtained by plotting daily K_{UVA}/K_S ratios versus the fraction of bright sunshine duration (Fig. 4B):

$$K_{UVA}/K_S = 0.0458 - 0.0113(n/N)$$
$$r^2 = 0.670$$
$$SE = 0.020 \qquad (9)$$

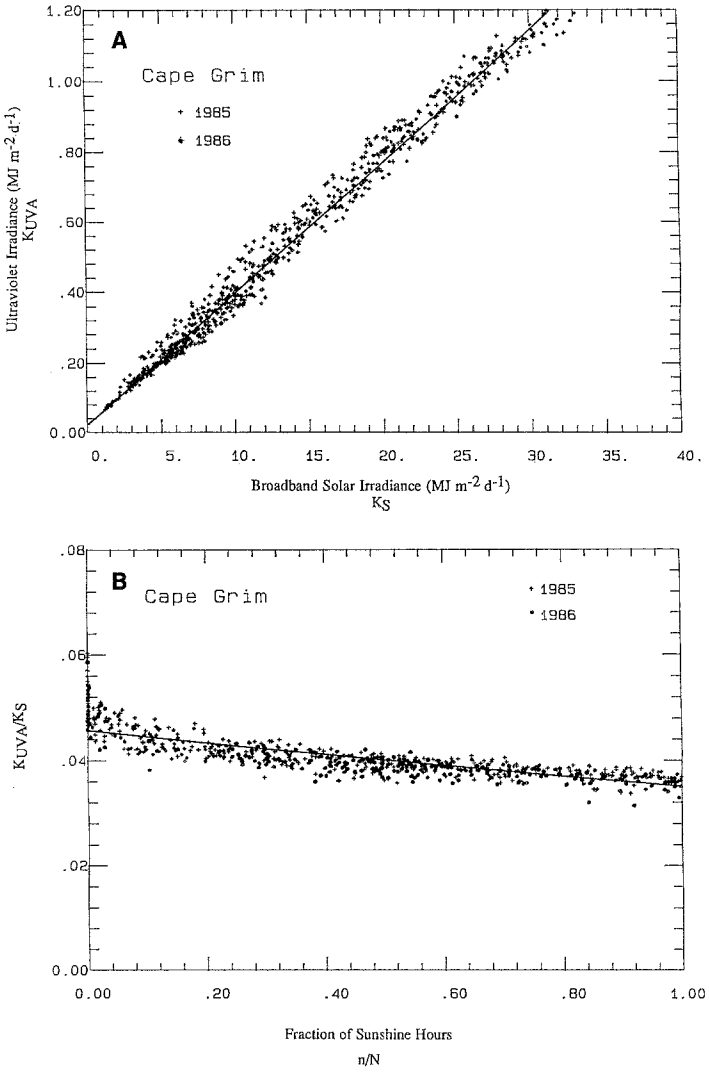

Fig. 4 **A** Relationship between measured daily global (K_S) and daily UV-A irradiance (K_{UVA}) for Cape Grim, Tasmania, Australia. Units are in MJ/m^2 per day. **B** Relationship between the ratio of measured daily UV-A to global irradiance (K_{UVA}/K_S) and the fraction of sunshine hours (n/N). Data for Cape Grim, Tasmania, Australia

where n is the actual sunshine duration and N is the maximum possible for that latitude and time of year. As cloud cover increases, n/N diminishes and the fraction of K_S that is in the UV-A region increases. These results agree qualitatively with the observations of Blumthaler and Ambach (1988) and Zavodska (1984). However similar relationships need to be developed in other environments to determine their general applicability.

Satellite approaches. Considerable effort has been devoted to the problem of mapping incoming broadband solar irradiance from satellites (Bahm 1981; Gautier et al. 1980; Moser and Raschke 1983). The benefits are considerable including access to low cost, timely and spatially uniform data on atmospheric reflectivity which may be related to cloud cover. In Australia, data from the geostationary meteorological satellite (GMS) has

been used to map daily solar irradiance on a regional scale of several hundred kilometres (Nunez 1988, 1990a). A simple physical relationship is used to calculate K_S:

$$K_S = K_E (1-\alpha_A)(1-\phi_A) \quad (10)$$

where K_E is the extra-terrestrial daily irradiance above the pixel of interest, ϕ_A is a daily absorption term obtained from precipitable water vapour measurements, and α_A is a daily atmospheric reflectance term. Essentially the satellite-determined reflectivity in the visible band, which varies from pixel to pixel with cloud cover, is related to α_A using a reflectance model.

From Eqs. 8 and 10, it is possible to estimate UV-A irradiance at time scales of a day or longer and on regional to continental spatial scales. The high frequency limit of one day is established by the three daily scans of GMS, although in theory the technique may be applicable to estimate hourly irradiances. The regional scale is appropriate since the satellite reflectivity information is limited by the satellite field of view (1.25 km × 1.25 km in the visible band at the equator and 140° E. To illustrate the technique, Eq. 8 was applied to a satellite-derived solar irradiance map for the region surrounding Hobart, Tasmania. As part of a previous study (Nunez 1990), monthly average solar irradiances were estimated for 2° by 2° regions surrounding every Australian capital city. Each irradiance map would contain a theoretical maximum of 279 images (3 daily images × 31 days × 3 years) used in the derivation of a monthly average figure estimated over 3 years. In actual fact the available images were less than the optimum value due to reception and data processing difficulties.

Figure 5 shows the resultant pattern of UV-A irradiance for the month of January in southeastern Tasmania. The standard error in the estimate of K_S (Eq. 10) is 0.41 MJ/m^2 per day, and in the estimate of K_{UVA} (Eq. 8) it is 0.035 MJ/m^2 per day. It may be shown that these two errors translate into a standard error of about 0.060 MJ/m^2 per day in the overall estimation of K_{UVA} using Eqs. 8 and 10. As a result an interval of 0.05 MJ/m^2 per day has been chosen in the display of the grey levels in Fig. 5.

The resultant pattern shows lowest UV-A irradiances (0.60–0.64 MJ/m^2 per day) in the cloudy southwest portion of the State, and increasing to highest values (0.80–0.84 MJ/m^2 per day) in the Central Midlands and on the East Coast. Given the linear expression between the K_{UVA} and K_S exhibited in Eq. 8, Fig. 5 presents no new information regarding resultant patterns. Its usefulness lies in the estimation of absolute levels of UV-A irradiance which may then be applied to determine biological impact. This technique may be used in any environment which may have pyranometer and/or satellite-derived solar irradiance data provided Eq. 8 is tested for local applicability.

The case for UV-B radiation is more complex due to the high levels of ozone absorption occurring in this band. As a result, a linear relationship between a narrowband and a broadband value such as shown in Eq. 8 would not be applicable. The approach that may be followed (Nunez 1990b) consists in developing an empirical relationship between the daily cloudy sky transmissivity (T_{UVB}) and a satellite-derived cloudiness index. The following relationship was derived for Melbourne, Victoria, Australia (37°49″ S; 145° E):

$$T_{UVB} = \left[\frac{K}{K_0}\right] = 1.03 - 0.19\,C - 0.18\,[C_0]^2 - 0.14\,C_3 + 5.3\times10^{-2}\,[C_3]^2 - 0.59\,C_6 + 0.31\,[C_6]^2 \quad (11)$$

Daily UV-B irradiances $(K)_{UVB}$ were obtained with an International Light Il 1700 radiometer consisting in an SED 240 solar blind vacuum photodiode and an NS297 filter with half power points of 288 nm and 300 nm. The instrument was recalibrated against a SPEC 180B double grating monochromator spectrometer to yield an

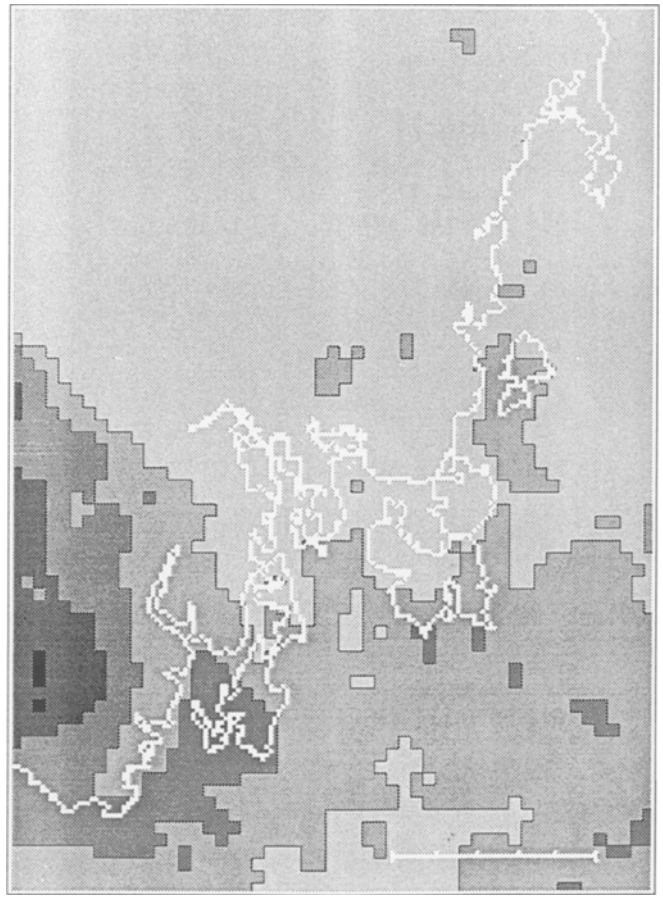

Fig. 5 Mean daily UV-A irradiance (in MJ/m^2 per day × 10) for the Hobart region for the month of January. The image represents a 2° × 2° region with Hobart airport at its geometric centre. A distance scale with 10 km intervals is shown. ■ 6.0–6.4; ■ 6.5–6.9; ■ 7.0–7.4; ■ 7.5–7.9; ■ 8.0–8.4

integrated irradiance in the wavelength range 280 nm to 315 nm. Concurrent with these measurements, daily ozone data from the TOMS spectrometer aboard Nimbus-7 were collected for the Melbourne region along with three daily visible digital images from GMS, also for the same region. The data set encompassed the period 1 September 1986 to 31 December 1987.

A daily clear sky irradiance $(K_0)_{UVB}$ was obtained using the model of Green et al. (1980) with the ozone data. The model gave an RMS difference (measured − model) which was 9.5% of the mean measured value when tested against measurements for 32 cloudless days. Cloud cover for the hours of 0, 3 and 6 Greenwich Mean Time (GMT) (C_0, C_3 and C_6) was obtained using the relationship:

$$C_i = \frac{\alpha_i - (\alpha_{min})_i}{(\alpha_{max})_i - (\alpha_{min})_i} \quad (12)$$

where C_i is a normalised cloud index obtained at times $i = 0$, 3, 6 GMT; α_i is the satellite reflectivity at time i; and $(\alpha_{min})_i$, $(\alpha_{max})_i$ are the minimum and maximum reflectivities for time i respectively. A minimum reflectivity $(\alpha_{min})_i$ was obtained by searching through all the images comprising the average and selecting, for each pixel, a minimum reflectivity value. This procedure ensures that localised effects such as surface cover type and texture are taken into account. By contrast, a maximum reflectivity $(\alpha_{max})_i$ is mostly dependent on cloud type and thickness. As a result a single value was obtained based on all records for the study period. This value was assumed to apply for all three GMT times with satellite data.

Equation 11 represents the results of a multiple linear regression between T_{UVB} as the dependent variable and C_0, C_3 and C_6 as independent variables. Data were obtained for Yallambie during the period 1 November 1986 to 28 February 1987 and much scatter was obtained for the daily relationship ($r^2 = 0.55$, SE of estimate = 0.16). Equation 11 was then used to calculate K_{UVB} on an independent data set encompassing the period 1 November 1987 to 31 December 1987. Daily RMS differences were 7.2 KJ/m^2 per day corresponding to 20.7% of the mean measured value. Averaging the K_{UVB} estimates over weekly periods reduces the RMS differences to 4.1 KJ/m^2 per day, or 11.1% of the mean value. Figure 6 presents a scatter plot of the calculated weekly average UV-B irradiances versus measured values.

In mapping applications, K_{UVB} was estimated from Eq. 11:

$$K_{UVB} = (K_0)_{UVB} \times F(C_0, C_3, C_6) \quad (13)$$

where F is the multiple linear regression function (Eq. 11). The clear sky value, $(K_0)_{UVB}$ was derived for Yallambie and was assumed to be representative of the entire Melbourne region. Cloud cover C_0, C_3 and C_6 was derived from the satellite data and varies with every pixel. Figure 7 presents the daily average irradiance for the period 1 November to 20 November 1986. Of interest is the lower range across the centre of the image, and the higher range north and south. The variability is considerable and is undoubtedly a result of orographic clouds to the north of Melbourne. Drier conditions prevail at the north end of the image as moisture-bearing frontal systems are not as common here.

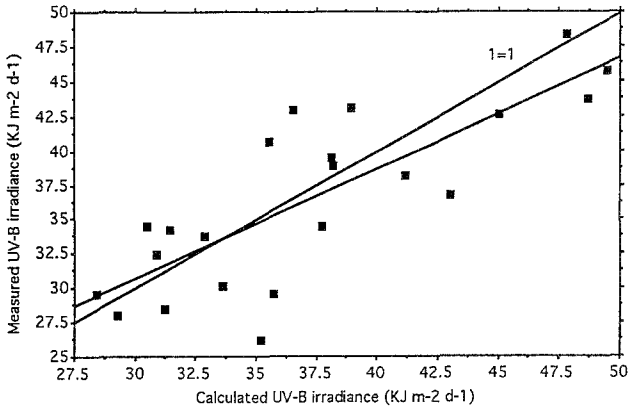

Fig. 6 Plot of weekly average measured versus calculated UV-B irradiances. Data are for Yallambie, Victoria, Australia. Also shown is the 1 = 1 line. Linear regression between the two yielded: {Measured} = 6.704 + 0.798 {Calculated}; $r^2 = 0.614$; estimated SE = 3.96. Units are in KJ/m^2 per day

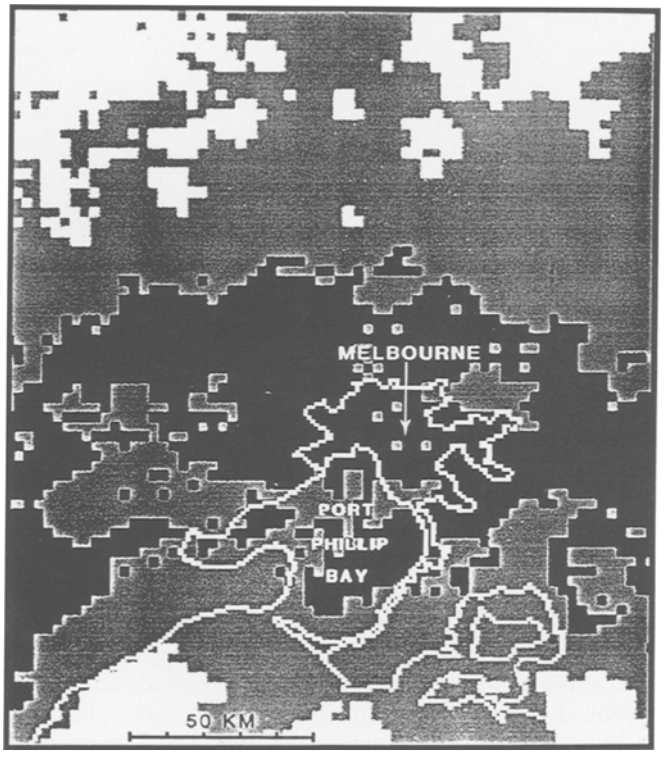

Fig. 7 Mean daily UV-B erythemal irradiance for the Melbourne region for the period 1 November to 20 November 1986. Units are in KJ/m^2 per day. The image represents a 2° × 2° region with Tullamarine Airport at its geometric centre. A distance scale with 10 km intervals is shown. KJ m^{-2} d^{-1}: ■← 20.0–24.9; ▩← 25.0–29.9; □← 30.0–34.9

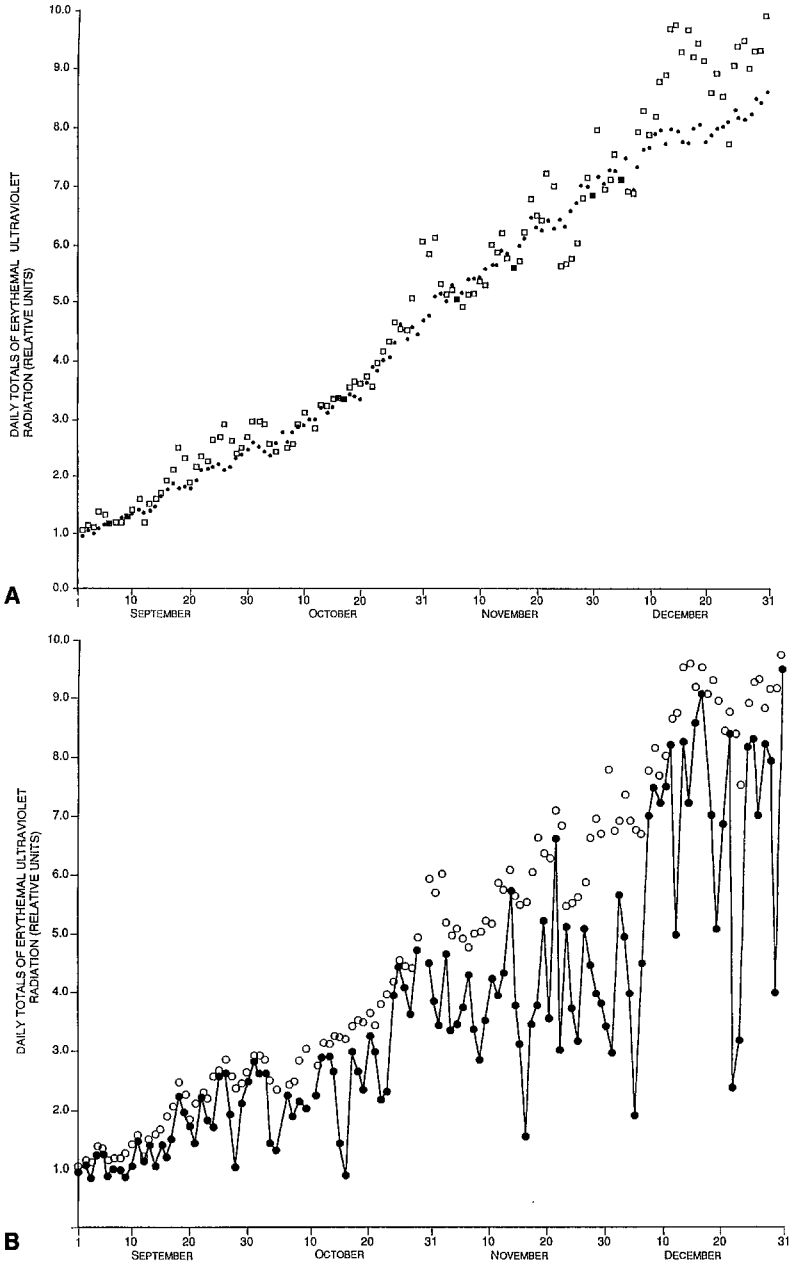

Fig. 8 **A** Ten year daily means (*black circles*) and daily totals for 1987 (*white squares*) of UV-B erythemal irradiance for cloudless conditions at Hobart Airport. Data normalised to 1 September 1987. **B** Daily total erythemal UV-B irradiance for cloudless conditions (*white circles*) and cloudy conditions (*black circles*). Data normalised to 1 September 1987. **A** ● 10 Year average (1979–1988); □ daily totals for 1987. **B** ○ Cloudless conditions 1987; ● including cloud cover 1987

To illustrate the importance of cloud cover in the ozone depletion problem, some model calculations of surface erythemal irradiance have been estimated for Hobart, Australia. Ten years of daily ozone data for the Hobart region were obtained from the TOMS radiometer aboard Nimbus-7. Only data from September 1 to December 31 were available for each year from 1979 to 1988. The last year of available data, 1988, comprised the period from September 1 to November 9. The model of Green et al. (1974) was used to calculate daily irradiances in the erythemal band for this time period using the TOMS ozone data and for cloudless conditons. Figure 8A presents two time series. The black circles represent the average irradiance for each day of the year. Each data point represents an average over 10 years of data (for example September 10, 1979; September 10 1980; September 10, 1981 ...). All data are then normalised by the irradiance on September 1, 1979. The open squares represent normalised data for 1987 only.

As expected, both time series undergo a marked change from September 1 to December 31. The 1987 data appear higher on average, with periods lasting for several days which are between 10 and 20% higher than the mean. The strong increase in erythemal UV-B radiation during December 1987 has been attributed to a northward migration of ozone-deficient air from the Antarctic region (Atkinson et al. 1989). A sample student's t-test performed on the daily difference (1987 − mean) resulted in a highly significant increase in the 1987 figures compared with the previous decade averages.

Figure 8B presents the daily irradiance for both cloudless and cloudy conditions. The data for cloudy conditions have been obtained using the cloud trans-

missivity relationships of Barton and Paltridge (1979; see also Fig. 2) with three-hourly cloud data for Hobart Airport. The dominant influence of cloud cover can be observed. It is feasible that prolonged periods of drought or high rainfall would bring changes in erythemal radiation that were much higher or lower respectively than the mean and certainly higher than the present changes associated with ozone deficiencies.

It must be emphasised that there are scale problems when relating satellite-derived cloud data to surface radiometric measurements. For example, errors arise from the comparison of a point measurement (radiometer) with a spatially derived quantity (satellite cloud cover). However, if the cloud field structure appears 'frozen' in time and simply is transported in the pyranometer field of view, then good agreement will result in the two set of measurements following temporal averaging. Errors may arise when this condition is not met or may be due to other causes such as non-lambertian cloud reflection, variability in aerosol load, satellite sensor deterioration, etc. Despite these problems, satellite data are useful in that they may provide the only cloud-related information available at high spatial and temporal frequencies.

Discussion and conclusion

The field of ultraviolet radiation climatology is still at a very early stage of development. Despite this limitation, there is increasing demand for ultraviolet radiation data in relation to stratospheric ozone depletion. An important consideration that must be addressed is the lack of measurement standards. Unlike broadband pyranometers, which may be purchased as thermopile junctions (with a flat wavelength response) and referenced to a world radiation standard, there is no similar instrument covering the ultraviolet region. There is very little radiant energy in this region for the efficient operation of thermopile devices and solid state detectors must therefore be used for greater sensitivity. Unfortunately their response is wavelength-dependent and broadband measurements with solid state devices are difficult to interpret due to the changing spectra of solar radiation. Double grating spectrometers, when properly calibrated, offer the required high-quality spectral information. However these are costly and not easy to use by the average semi-skilled weather observer.

A more practical approach involves broadband solid state detectors with a narrow band filter. Choice of the band must ultimately come from the biological and medical experts who will use the data; at present their interests appear to focus on the three action spectra of erythema or human skin, plant damage and DNA damage. The Robertson-Berger meter mimics the human skin response and is widely used. However a considerable calibration effort appears necessary if accurate, reliable readings are needed and it is suggested that a suitable instrument standard be developed to cover the erythema region. Polysulphone badges perform a useful task in assessing individual human loads. The challenge would appear to lie in relating these measurements to the radiometer measuring horizontal irradiance. Studies of this nature would be a useful step in the development of radiation climatologies applicable to humans.

A variety of spectral models have been presented in the literature covering a multitude of approaches ranging from multi-layer delta Eddington radiative transfer schemes to two stream approximations and to semi-empirical models. It is difficult to give an overall assessment and comparison of the different models since there is no comprehensive measurement network to test their global applicability and generality. Theoretical schemes perform a crucial role in defining the sensitivity of the surface irradiance to the various atmospheric constituents. Ultimately these results must be exported into simpler schemes of semi-empirical parameterisation for use in climatology and by non-specialists. In carrying out the transfer it is important that an aerosol parameterisation be included (for example, by use of visibilities) since this parameter will strongly affect the character of the surface irradiance. It appears that further development is needed in this area.

Mapping of the surface irradiance field involves an assessment of cloud effects. Theoretical models reveal that cloud transmissivities are largely wavelength-independent in the UV-A region, but appear to exhibit lower transmissivities in most of the UV-B region. Both theoretical and experimental studies show a strong dependence of transmissivity on cloud type. There is a need to develop physical models of surface irradiance which also include cloud type transmission. It is likely that this modification will include an improved performance over models which do not include cloud type (Eq. 7).

In the absence of surface observations of cloud data, a satellite approach may be adopted. The technique is characterised by large errors compared to surface measurements on a daily time scale or less. However, given the random nature of cloud distribution, better results are obtained by weekly averaging. Other sources of error include non-lambertian reflection of solar radiation from clouds and localised aerosol loads (Nunez 1990a, 1993). For these reasons it would appear advantageous to calibrate the technique using local surface radiation measurements.

To conclude, it should be emphasised that ultraviolet radiation climatology is needed to assess properly the effect of ozone depletion on the biosphere. Such climatology relies on models which accurately replicate the depletion of radiation by all the atmospheric components including ozone, aerosols and cloud cover. The greatest challenge lies in acquiring information on cloud depletion and it is suggested that satellite techniques could prove very valuable for this purpose. Model estimates will also need to be validated against a comprehensive and reliable network of surface instrumentation.

Acknowledgements The authors gatefully acknowledge the assistance provided by Geoffrey Day for data processing and Robert Slack for the drawings. The ozone data were provided by Dr. A.J. Fleig, Dr. A.J. Krueger (NASA/GSFC), members of the TOMS Nimbus experiment and ozone processing teams and the National Space Science Data Centre through the World Data Centre – A for Rockets and Satellites.

References

Angell JK, Korshover J, Planet WG (1985) Ground-based and satellite evidence for a pronounced total-ozone minimum in early 1983 and responsible atmospheric layers. Month Weather Rev 113:641

Atkinson RJ, Matthews WA, Newman PA, Plumb RA (1989) Evidence of the midlatitude impact of Antarctic ozone depletion. Nature 340:290

Bahm RJ (ed) (1981) Satellites and Forecasting of Solar Radiation. Proceedings of the First Workshop on Terrestrial Solar Resource Forecasting and on Use of Satellites for Solar Resource Assessment, 2–5 February 1981, Washington, DC. Publication Office, American Section of Solar Energy Society

Baker-Blocker A (1980) The effect of sunshine, cloudiness and haze on received ultraviolet radiation in New York. J Appl Meteorol 19:889

Baker-Blocker A, DeLuisi JJ, Dutton E (1984) Received ultraviolet radiation at the South Pole. Solar Energy 32:659

Barton IJ, Paltridge GW (1979) The Australian climatology of biologically effective ultraviolet radiation. Aust J Dermatol 20:68

Basher RE (1987) The calculation of solar ultraviolet radiation and its sunburning effect under clear skies. Scientific Report 26, New Zealand Meteorological Service

Berger DS (1976) The sunburning ultraviolet meter: design and performance. Photochem Photobiol 24:587

Berger DS, Urbach F (1982) A climatology of sunburning ultraviolet radiation. Photochem Photobiol 35:187

Berner P (1964) Investigation on the influence of clouds on ultraviolet sky radiation. Contract AF 61(052)-618, Technical Note 3. Physikalisch-Meteorologisches Observatorium Davos, Davos-Platz, Switzerland

Berner P (1972) Approximate values of intensity of natural ultraviolet radiation for different amounts of oyone. Final Technical Report. European Research Office, US Army, London. Contract No. DAJA 37-68-C-1017

Blumthaler M, Ambach W (1988) Human solar ultraviolet radiant exposure in high mountains. Atmos Envir 22:749

Borkowski J, Chai AT, Mo T, Green AES (1974) Cloud effects on middle ultraviolet global radiation. Acta Geophys Pol 25:287

Braslau N, Dave JV (1973a) Effect of aerosols on the transfer of solar energy through realistic model atmospheres. J Appl Meteorol 12:601

Braslau N, Dave JV (1973b) Effect of aerosols on the transfer of solar energy through realistic model atmospheres, Part II: Partly absorbing aerosols. J Appl Meteorol 12:616

Caldwell MM, Camp LB, Warner CW, Flint SD (1986) Action spectra and their key role in assessing biological consequences of solar UV-B radiation change. In: Worrest RC, Caldwell MM (eds) Stratospheric ozone reduction, solar ultraviolet radiation and plant life. Springer, Berlin p 87

Crutzen PJ, Isaksen ISA, Reid GC (1975) Solar proton events: stratospheric sources of metric oxide. Science 189:457

Dave JV, Halpern P (1976) Effects of changes in ozone amount on the ultraviolet radiation received at sea level of a model atmosphere. Atmos Envir 10:547

Davies JA, Schertzer WS, Nunez M (1975) Estimating global solar radiation. Bound Layer Meteorol 9:33

Davis A, Deane GHW, Diffey BL (1976) Possible dosimeter for ultraviolet radiation. Nature 261:169

Drummond AJ, Wade HA (1969) Instrumentation for the measurement of solar ultraviolet radiation. In: Urbach F (ed) The biological effects of ultraviolet radiation. Pergamon Press, Oxford, p 391

Farman JC, Gardiner BG, Shanklin JD (1985) Large losses of total ozone in Antarctica reveal seasonal ClO_xNO_x interaction. Nature 315:207

Farmer CB, Toon GC, Schaper PW, Blavier JF, Lowes LL (1987) Stratospheric trace gases in the spring 1986 Antarctic atmosphere. Nature 329:126

Fraser PJ (1989) Chlorofluorocarbons and stratospheric ozone. Chemistry in Australia, 56:272

Frederick JE, Alberts AD (1991) Prolonged enhancement in surface ultraviolet radiation during the Antarctic spring of 1990. Geophys Res Lett 18:1869

Frederick JE, Lubin D (1988) The budget of biologically active ultraviolet radiation in the earth-atmosphere system. J Geophys Res 93 (D4):3825

Frederick JE, Snell HE (1990) Tropospheric influence on solar ultraviolet radiation. J Climate 3:373

Gautier C, Diak G, Masse S (1980) A simple physical model to estimate incident solar radiation at the surface from GOES satellite data. J Appl Meteorol 19:1005

Grainger RG, Basher RE, McKenzie RL (1993) UV-B Robertson-Berger meter field calibration. Appl Optics (in preparation)

Green AES, Mo T, Miller JH (1974a) A study of solar erythema radiation doses. Photochem Photobiol 20:473

Green AES, Sawada T, Shettle EP (1974b) The middle ultraviolet reaching the ground. Photochem Photobiol 19:251

Green AES, Cross KR, Smith LA (1980) Improved analytic characterization of ultraviolet skylight. Photochem Photobiol 31:59

Halpern P, Dave JV, Braslau N (1974) Sea level sole radiation in the biologically active spectrum. Science 186:1204

Hofmann DJ, Oltmans SJ, Harris JM, Solomon S, Deshler T, Johnson BJ (1992) Observation and possible causes of new ozone depletion on Antarctica in 1991. Nature 359:283

Hollows F (1989) Ultraviolet radiation and eye diseases. Trans Menzies Found 15:113

Ilyas M (1987) Effect of cloudiness on solar ultraviolet radiation reaching the surface. Atmos Envir 21:1483

Ilyas M, Barton IJ (1983) Surface dosage of erythemal solar ultraviolet radiation near the equator. Atmos Envir 17:2069

Iqbal M (1983) An introduction to solar radiation. Academic Press, London

Kok CJ, Chalmers AN, Hengstberger F (1978) Measurements of the middle ultraviolet at Durban. Atmos Envir 12:1119

Lehman P, Karoly DJ, Newman PA, Clarkson TS, Matthews WA (1992a) Long-term winter total ozone changes at Macquarie Island. Geophys Res Lett 19:1459

Lehman P, Karoly DJ, Newman PA, Clarkson TS, Matthews WA (1992b) An investigation into the causes of stratospheric ozone loss in the southern Australasian region. Geophys Res Lett 19:1463

Liu SC, McKeen SA, Madronich S (1991) Effect of anthropogenic aerosol on biologically active ultraviolet radiation. Geophys Res Lett 18:2265

Lubin D, Frederick JE (1989) Measurements of enhanced springtime ultraviolet radiation at Palmer Station, Antarctica. Geophys Res Lett 16:783

Lubin D, Frederick JE (1990) Column ozone measurements from Palmer Station, Antarctica: variations during the Austral spring of 1988 and 1989. J Geophys Res 95(D9):13883

Madronich S (1992) Implications of recent total atmospheric ozone measurements for biologically active ultraviolet radiation reaching the earth's surface. Geophys Res Lett 19:37

McKenzie RL, Matthews WA, Johnston PV (1991) The relationship between erythemal UV and ozone derived from spectral irradiance measurements. Geophys Res Lett 18:2269

McKinlay AF, Diffey BL (1987) A reference action spectrum for ultraviolet induced erythema in human skin. Commission Internationale de l'Eclairage (CIE) Journal 6:17

Meador WE, Weaver WR (1980) Two stream approximations to radiative transfer in planetary atmospheres: a unified descrip-

tion of existing methods and a new improvement. J Atmos Sci 37:630
Mo T, Green AES (1974) A climatology of solar erythema dose. Photochem Photobiol 20:483
Moser W, Raschke E (1983) Determination of global radiation and of cloudiness from METEOSAT imaging data. Ann Meteorol (Neue Folge) 18:161
Nack MI, Green AES (1974) Influence of clouds, haze and smog on the middle ultraviolet reaching the ground. Appl Optics 13:2405
Nunez M (1988) A comparison of three approaches to estimate daily totals of global solar radiation in Australia using GMS data. Aust Meteorol Mag 36:25
Nunez M (1990a) Solar energy statistics for Australian capital regions. Solar Energy 44:343
Nunez M (1990b) Mapping ultraviolet radiation in the Australian region. 59th ANZAAS Congress, Hobart, 14–16 February 1990, Univ. Tasmania Printers, Hobart
Nunez M (1993) The development of a satellite-based insolation model for the tropical western Pacific Ocean. Int J Climatol 13:607
Paltridge GW, Barton IJ (1978) Erythemal ultraviolet radiation distribution over Australia: the calculations, detailed results and input data. CSIRO Division of Atmospheric Research Technical Paper 33
Rao CR, Takashima UT, Bradley WA, Lee TY (1984) Near ultraviolet radiation at the earth's surface: measurement and model comparisons. Tellus 36B:286
Reiter R, Munzert K, Sladkovic R (1982) Results of 5-year concurrent recordings of global, diffuse and UV-radiation at three levels (700, 1800, and 3000 m a.s.l.) in the Northern Alps. Arch Meteorol Geophys Biokl B30:1
Roberts A (1991) Human exposure to ultraviolet radiation under all sky conditions in Hobart, Tasmania. Thesis, Department of Geography and Environmental Studies, University of Tasmania
Rodskjer N (1983) Spectral daily insolation at Uppsala, Sweden. Arch Meteorol Geophys Bioclimatol B33:99
Roy C, Gies PH, Elliott G (1989) The ARL solar ultraviolet radiation measurement programme. Trans Menzies Found 15:71
Rundel R (1986) Computation of spectral distribution and intensity of solar UV-B radiation. In: Worrest RC, Caldwell MM (eds) Stratospheric ozone reduction, solar ultraviolet radiation and plant life. Springer, Berlin, p 49
Schippnick PF, Green AES (1982) Analytical characterization of spectral actinic flux and spectral irradiance in the middle ultraviolet. Photochem Photobiol 35:89
Scotto J, Fears TR (1987) The association of solar ultraviolet and skin melanoma incidence among caucasians in the United States. Cancer Invest 5:275
Scotto J, Cotton G, Urbach F, Berger D, Fears T (1988) Biologically effective ultraviolet radiation: surface measurements in the United States, 1974 to 1985. Science 239:762
Seckmeyer G, McKenzie RL (1992) Increased ultraviolet radiation in New Zealand (45 deg S) relative to Germany (48 deg N). Nature 359:135
Setlow RB (1974) The wavelength in sunlight effective in producing skin cancer. Proc Natl Acad Sci 71:3363
Shettle EP, Green AES (1974) Multiple scattering calculation of the middle ultraviolet reaching the ground. Appl Optics 13:1567
Spinhirne JD, Green AES (1978) Calculation of the relative influence of cloud layers on received ultraviolet and integrated solar radiation. Atmos Envir 12:2449
Stolarski RS, Krueger AJ, Schoeberl MR, McPeters RD, Newman PA, Alpert JC (1986) Nimbus 7 satellite measurements of the springtime Antarctic ozone decrease. Nature 322:808
Stolarski RS, Bloomfield P, McPeters RD (1991) Total ozone trends deduced from Nimbus 7 TOMS data. Geophys Res Lett 18:1015
Vogelmann AM, Ackerman TP, Turco RP (1992) Enhancement in biologically effective ultraviolet radiation following volcanic eruptions. Nature 359:47
Webb A, Steven MD (1984) Measurement of solar UVB radiation in the English midlands. Arch Meteorol Biophys Bioclimatol B35:221
Webb A, Steven MD (1986) Daily totals of solar UVB radiation estimated from routine meteorological measurements. J Climatol 6:405
Worrest RC (1982) Review of literature concerning the impact of UV-B radiation on marine organisms. In: Calkins J (ed) The role of solar ultraviolet radiation in marine organisms. Plenum Press, New York, p 429
Zavodska E (1984) The effects of cloudiness, sunshine and snow cover on ultraviolet radiation at Skalnate Pleso. Contrib Geophys Inst Slovak Acad Sci Ser Meteorol 5:21
Zigman S (1977) Near UV light and cataracts. Photochem Photobiol 26:437